3D seismic imaging of a Tertiary Dyke Swarm in the Southern North Sea, UK

Mostyn Wall,* Joe Cartwright,* Richard Davies† and Andrew McGrandle‡

*3DLab, School of Earth, Ocean and Planetary Sciences, Cardiff University, Park Place, Cardiff CF10 3YE, UK
†CeREES, (Centre for Research into Earth Energy Systems) Department of Earth Sciences, University of Durham, Science Labs, Durham DH1 3LE, UK
‡Ark Geophysics, 1 Mercers Manor Barns, Sherington, Newport Pagnell MK16 9PU, UK

ABSTRACT

We use three-dimensional (3D) seismic reflection and magnetic data to interpret and describe the 3D geometry of igneous dykes in the southern North Sea. The dykes were emplaced into Paleozoic and Mesozoic sediments and have a common upper termination in Early Tertiary sediments. We interpret the dykes to be part of the British Tertiary volcanic province and estimate the age of the dykes to be 58 Ma. The dykes are characterized by a narrow 0.5–2 km wide vertical disturbance of seismic reflections that have linear plan view geometry. Negative magnetic anomalies directly align with the vertical seismic disturbance zones and indicate the presence of igneous material. Linear coalesced collapse craters are found above the dykes. The collapse craters have been defined and visualized in 3D. Collapse craters have formed above the dyke due to the release of volatiles at the dyke tip and resulting volume loss. Larger craters have potentially formed due to explosive phreatomagmatic interaction between magma and pore water. The collapse craters are a new Earth analogue to Martian pit chain craters.

INTRODUCTION

Magmatic intrusion into the upper crust is an important process in sedimentary basins (duToit, 1920; Planke *et al.*, 2005 and Cartwright, 2007). The understanding of igneous sill and dyke intrusions and their interaction with basin processes have been extensively documented using outcrop mapping (duToit, 1920; Novikov & Slobodskoy, 1978; Kokelaar, 1982; Lorenz, 1986; Chevallier & Woodford, 1999; Nemeth *et al.*, 2001 and Goulty, 2005). Three-dimensional (3D) seismic reflection data provide a valuable scientific tool that have been proven to image and gain novel insights into new geological features not previously identified because of the scale and the lack of three-dimensionality of the vast majority of outcrops, (Davies *et al.*, 2004; Hansen *et al.*, 2004 and Cartwright, 2007). Magmatic intrusions into sedimentary basins have been extensively described in the North Sea, West of Shetland and the Norwegian Møre and Vøring basins using two-dimensional (2D) and 3D seismic reflection data, significantly advancing previous models that were based on outcrop studies (Hitchen & Ritchie, 1987, 1993; Skogseid *et al.*, 2000; Svensen *et al.*, 2003; Jamtveit *et al.*, 2004; Svensen *et al.*, 2004; Hansen & Cartwright, 2004, 2006; Trude, 2004; Planke *et al.*, 2005). Dykes have rarely been interpreted using 3D seismic reflection data due to problems in ima-

ging vertical bodies in the subsurface. In the southern North Sea dykes have only previously been interpreted using 2D seismic reflection data and magnetic modelling (Kirton & Donato, 1985; Brown *et al.*, 1994). In this paper we use 3D seismic reflection data to investigate dykes in the southern North Sea. The benefits of 3D seismic reflection data are that we can analyse the 3D spatial distribution and seismic characteristics of dykes and their relationship with surrounding sedimentary strata, allowing for a re-evaluation of the field based models and the previous 2D interpretation by Brown *et al.* (1994).

The principal aim of this paper is the use of 3D seismic interpretation supported by marine magnetic data to further the understanding of dyke emplacement into sedimentary basins and to document the 3D geometry of dykes found in the southern North Sea. We also investigate the relationship between dyke emplacement and subsequent folding and consider whether dyke emplacement has a control on fold development in the study area. Lastly, we examine collapse craters associated with the dykes and compare them with linear pit chain craters on Mars, proposing that they represent new analogues.

GEOLOGICAL SETTING

The southern North Sea is dominated by the development of the west–east trending southern Permian Basin (SPB), 140 km east of the UK coastline (Fig. 1).

Correspondence: Mostyn Wall, StatoilHydro ASA, NO-0246 Oslo, Norway. E-mail: mostynwall@hotmail.com
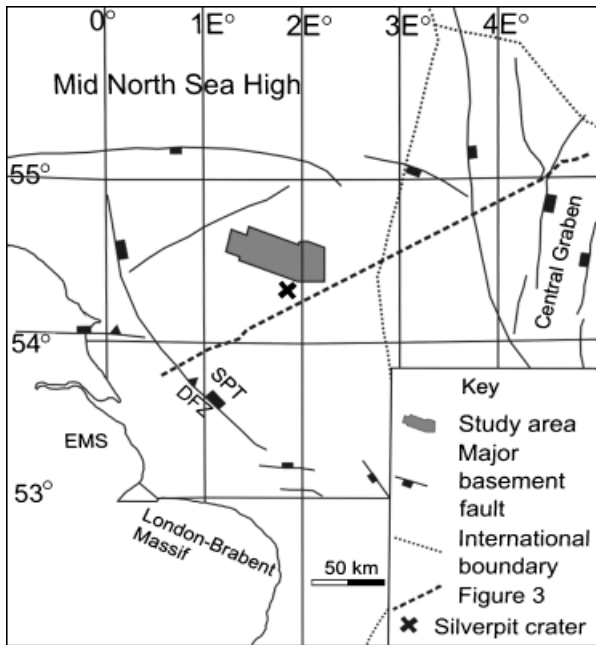
Fig. 1. Map showing the location of the Southern North Sea study area. Major basement faults and structures are highlighted, EMS, East Midlands shelf; DFZ, Dowsing Fault Zone. After Bailey *et al*. (1993) and Coward & Stewart (1995).

Fig. 2. Map showing Post Zechstein structures in the SNS. The major salt-cored anticlinal and synclinal troughs of Tertiary age in the SNS. Also shown is the peripheral graben system formed in the Early Cretaceous. DOGS, Dogger Graben System. Based on Van Hoorn (1987), Hughes & Davison (1993) and Coward & Stewart (1995).

The Permian Rotliegend and Zechstein Group sediments were deposited in a series of north–northwest striking grabens, potentially reactivating basement structures inverted during the Late Carboniferous (Coward, 1993). The east–west trend of the Permian basin continued to control sediment deposition up to the Middle Triassic when the Dowsing Fault Zone (DFZ), a major northwest–southeast (NW–SE) trending basement fault, began to influence sedimentation (Cameron *et al*., 1992).

The tilting of the basin during Jurassic times resulted in thickening of the Jurassic strata in the southwestern basin margin and erosion in northeastern part of the basin (Stewart & Coward, 1995) (Fig. 3). Late Jurassic wrench fault movements in the Sole Pit Basin resulted in regional uplift and deep truncation of the Jurassic and in places even of the Triassic series, creating a major regional unconformity, known as the Base Cretaceous unconformity (Ziegler, 1981) (Fig. 3).

Coward & Stewart (1995) produced a model for the post-Early Cretaceous basin evolution, identifying gravity spreading following inversion as the driving mechanism for the development of the post-salt structures. The post-Early Cretaceous history of the SPB basin is characterized by inversion, in terms of both basin tilt and reverse slip on individual faults (Van Hoorn, 1987; Coward & Stewart, 1995). The basin tilted to the northeast, a reversal of the Jurassic tilt direction (Coward & Stewart, 1995). The reversal of basin tilt is recorded in the thickening of the Tertiary sediments to the northeast (Fig. 3). Inversion of the basement structures produced a large wavelength forced fold above uplifted synrift sediments, together with shortening of the post-salt section in a series of buckle folds in the
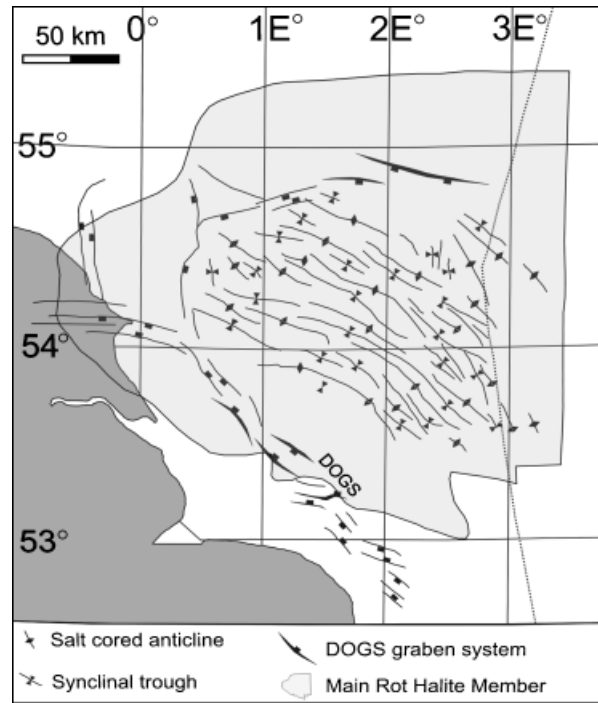
centre of the Sole Pit Basin. Inversion and the reversal of basin tilt also resulted in the uplifting of the thick sedimentary wedge in the Sole Pit Trough. Gravity spreading within the sedimentary wedge resulted in extensional faulting in the thickest part of the wedge (Dowsing Graben System) and shortening, in the form of detachment buckle folds, in the thinner peripheral zones (Silverpit Basin) (Coward & Stewart, 1995) (Figs 2 and 3). During the amplification of the folds in the SNS, buckle folds were supplemented by salt movement in response to differential sedimentary loading. During buckle fold growth, salt in the anticlinal core was moulded first into swells, then into pillows as the fold amplitude increased (Coward & Stewart, 1995).

Hughes & Davison (1993) dated the dominant phase of fold development and salt movement as being Eocene to Oligocene (33–28 Ma). Van Hoorn (1987) and Ziegler (1981) related the regional inversion and development of the salt cored folds to coincide with the main phase of Alpine orogeny in the Oligocene. Figure 2 illustrates the extent of the post-salt extensional and compressional structures in the SPB.

3 SEISMIC INTERPRETATION OF STUDY AREA

Database

The seismic dataset on which this paper is based is located in the Silverpit basin (Figs 1 and 3). The survey is time mi-
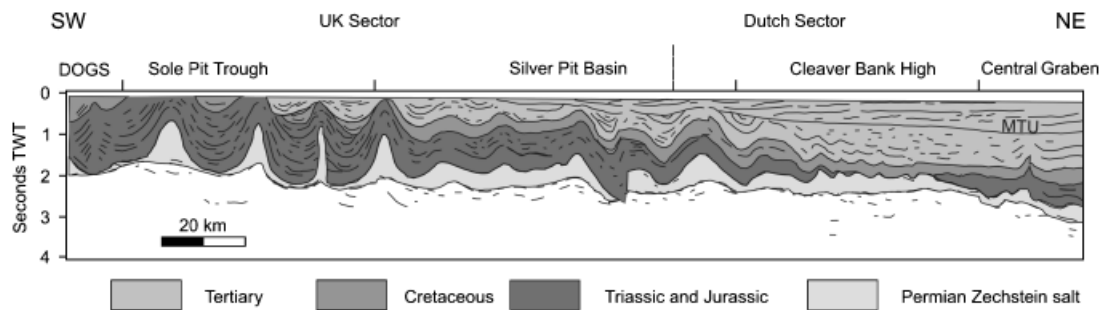
Fig. 3. Line drawing across the SPB basin annotated with structural domains. Vertical exaggeration approximately x5. Cretaceous Chalk is shaded, defining a wedge of Triassic and Jurassic whose geometry records Late Jurassic erosion. The Cretaceous is overlain by a second wedge of Tertiary sediments which thickens in the opposite direction, recording the reversal of the Jurassic basin tilt. The Mid-Tertiary unconformity (MTU) is a major unconformity across the SPB. TWT, two way time. Based after Stewart & Coward (1995). 174 × 48 mm.

grated and covers an area of approximately 1283 km² . In-lines and crosslines are spaced at 12.5 m. The phase of the data are close to a phase rotation of 90° wavelet and displayed using negative standard polarity (SEG standards) (Simm & White, 2002). An increase in acoustic impedance, as seen, for example, at the seabed and the reflection marking the top Cretaceous age Chalk group, is displayed as a wide trough (red) over a wide peak (black).

Structural elements

The Silverpit basin is a NW–SE trending Permian age basin that has inherited basement lineaments (George & Berry, 1997). A NW–SE trending fault can be identified in the pre-Zechstein Permian basement, forming part of a positive ridge in the basement that trends NW–SE (Fig. 5). The Zechstein Group overlies the basement and has a relatively horizontal base that is displaced by the NW–SE trending fault. The post-Zechstein strata are characterized by two major salt swells which are typical of the central part of the SPB basin (Figs 2–4). The Triassic and Jurassic strata decrease in thickness towards the northeast of the survey. Cretaceous age Chalk rocks exhibit a subtle variation in thickness across the survey area. An example of this is shown in Fig. 5B, where modest thickening of the Chalk occurs above the crest of a present day salt pillow/fold. This suggests possible rapid tectonic subsidence related to movement along basement faults or the overlap of salt withdrawal basins, where adjacent salt pillows/folds grew at different times (Hughes & Davison, 1993).

Two long wavelength folds are imaged in the survey trending NW–SE, similar to other long wavelength folds in the SPB (Figs 2, 3 and 5). The folds have a wavelength of 10 km. The fold axes trend NW–SE, tracing the underlying basement fault trend. Hughes & Davison (1993) note that there are numerous examples of basement faults which do and do not have pillows above them and that the spacing of pillows is probably independent of basement fault positions. The more south-westerly of the two fold axes has an offset geometry in the northwestern part of the survey area (Fig. 4).

Tertiary strata in the survey thicken towards the north due to uplift of the SPT to the southwest (Figs 3 and 4). The Mid-Tertiary unconformity can be seen in the survey near the seabed. Owing to uplift and development of the post-salt fold structures few Mid-Tertiary growth strata are preserved in the cores of the anticlines. The Mid-Tertiary unconformity is more pronounced regionally where thicker Tertiary sediments are truncated in the basin depocentre in the East (Fig. 3).

Two linear seismic disturbance zones (DZ) can be identified in the seismic reflection data trending NW–SE, located in the synclinal axes of the folds (Fig. 5).

Seismic DZ

Figure 5 shows three vertical seismic lines through the dataset. On each of the seismic lines two or more vertical zones of seismic reflection discontinuity can be identified, which we term seismic DZ, labelled A, B and C (Fig. 5). The DZ are vertical to sub-vertical columns characterized by a marked decrease in strength of seismic reflection amplitude compared to adjacent seismic reflections and in some cases by disruption of stratal reflections (Fig. 5). The DZ widths range from 0.5 to 2 km (Figs 5, 6 and 8). Two of the DZ are located in the troughs of the regional synclines and trend along their synclinal axes (Fig. 5). DZ width and character varies considerably along strike (Fig. 5). The DZ have a common upper stratigraphic limit in the Lower Tertiary, just above the high amplitude continuous seismic reflection marking the top of the Chalk, above which the seismic reflections are continuous (Fig. 6). The DZ can be identified down into the Permian Rotliegend strata, beneath which the seismic reflection resolution is significantly reduced. Seismic reflections can be traced across the DZ. A common feature of the DZ is the abrupt downward vertical shift of reflections within the DZ. The magnitude of the vertical shifts of the internal seismic reflections within the DZ are seen to be constant with depth (Fig. 6).

The lateral variation of DZ width and internal reflection geometry is seen throughout the dataset (Figs 6 and 8).
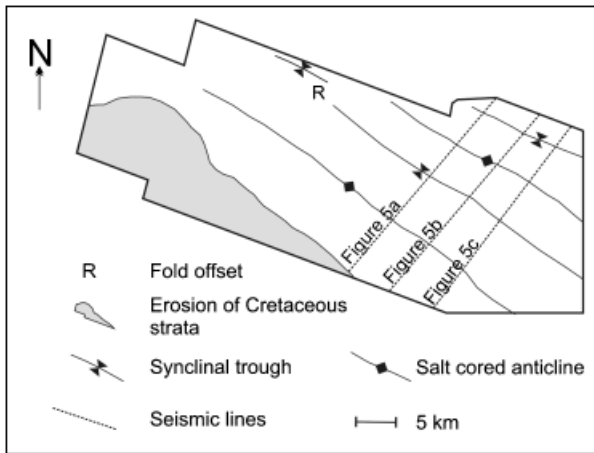
Fig. 4. Map of the seismic study area showing the Tertiary fold axes and erosion of the Cretaceous and Tertiary strata. Figure 5 seismic lines are highlighted.

Figure 6a shows a close up of a typical wide DZ from Fig. 5. The DZ is 1 km wide and consists of a central vertical seismic disturbance, (marked Q) and one vertical (marked X), and one sub-vertical seismic disturbance (marked Z), that mark the lateral boundaries of the DZ. Above the central vertical disturbance, in the Cretaceous age Chalk Group, is a downward tapering, broadly triangular high amplitude unit of seismic reflections (Fig. 6, marked HA). The seismic reflections in the lower part of the unit dip towards the upper stratigraphic tip of the central disturbance, (marked Q), and the upper reflections of this unit decrease in dip upwards, becoming horizontal at the top of the unit. Seismic reflections within the Chalk are truncated by the HA unit. The lateral seismic disturbances, marked X and Z, join up with the upper edges of the HA unit (Fig. 6).

Some of the DZ are characterized by a narrower seismic reflection disturbance. The reflections within the narrow DZ are displaced downwards and the reflections either side of the DZ can accurately be traced across the DZ (Fig. 6b). The narrower DZ do not contain internal seismic truncations or disruptions seen in the broader DZ (Fig. 6a and b).

The top of the DZ is characterized by depressions; the margins of which are marked by steep normal faults. The depressions are identified in the seismic reflections marking the top of the Chalk Group (Figs 6a, b and 8). The down-sagged reflections (Figs 6a, b and 8) are located above and below the continuous reflection marking the top of the Chalk Group. Subtle onlapping reflections are found within the depression above the top Chalk seismic reflection and a thickening of strata is observed above the down-sagging reflections (Figs 6a, b and 8). The onlapping reflections within the depression are most likely Tertiary siliclastics onlapping onto Cretaceous Chalk. The DZ is spatially related to the overlying depression. Where the depression is narrow, the underlying DZ is narrow; where the depression is wide the underlying DZ is wide (Figs 6 and 8).
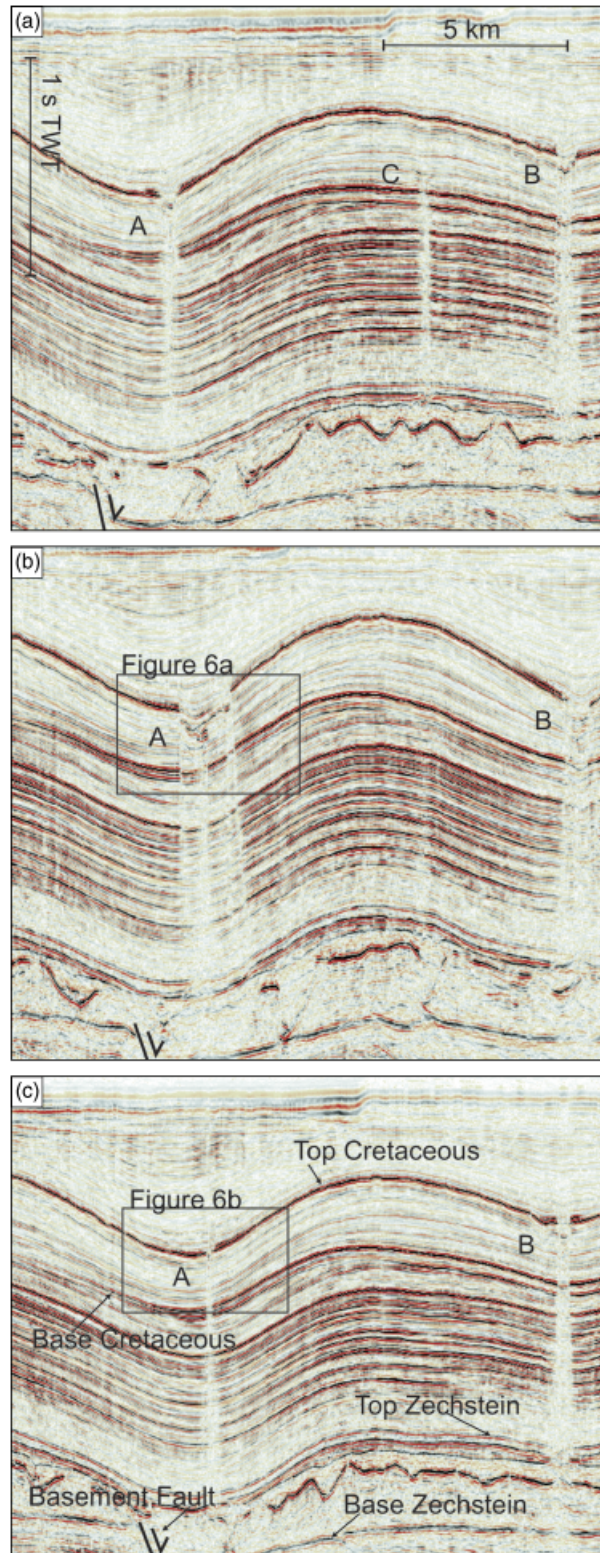

Fig. 5. Seismic lines across the survey, perpendicular to the trend of the DZ, showing the vertical seismic characteristics of the disturbance zones (DZ). (a) Seismic line showing the location of the dykes. A, B and C correspond to DZ and dyke location. Dyke C is only identified in this seismic line. (b) Adjacent seismic line showing the variation in DZ width. (c) The main stratigraphic seismic reflection markers are highlighted. The DZ width is considerably thinner than the previous examples.
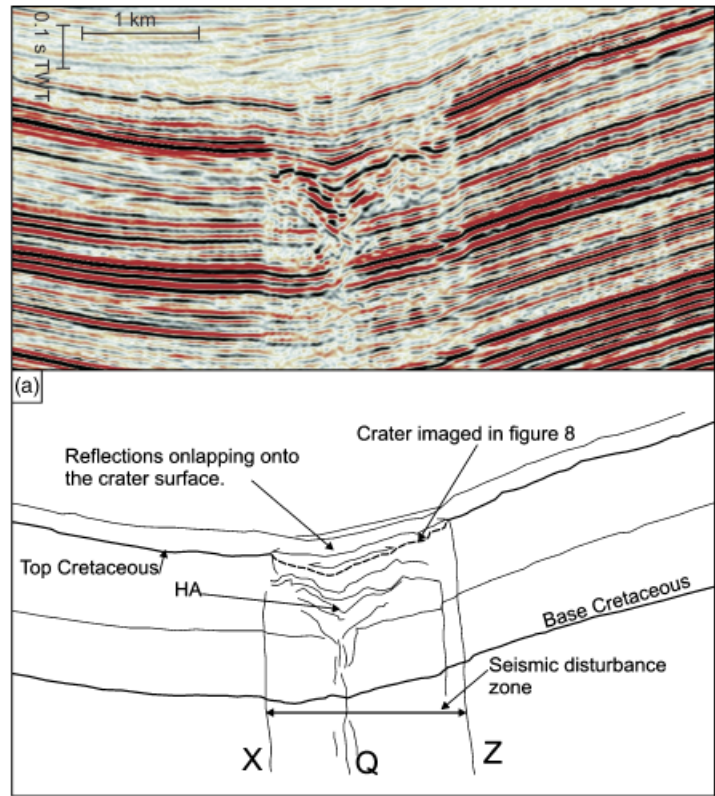
Fig. 6. Close up of the upper area of a DZ and a seismic line drawing showing the main features. (a) Seismic line through a wide DZ, HA, high amplitude unit, Q, central vertical disturbances, X and Z, lateral vertical disturbances. The internal Chalk seismic reflections truncate against the HA unit. Drape of reflections can be seen above the top Chalk reflection. (b) Seismic line through a thin DZ.
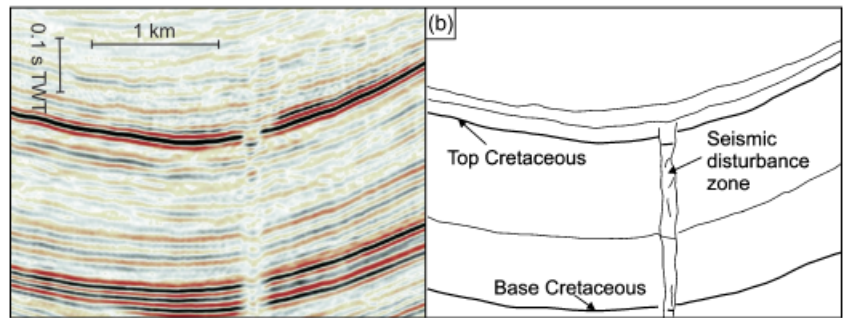
The high amplitude top Chalk seismic reflection provides an excellent surface to map the depressions above the DZ. The top Chalk surface map of the depressions shows a crater like geometry (Figs 7 and 8). Three linear NW–SE-orientated crater chains can be identified from the resulting top Cretaceous age map (Fig. 7). The largest linear chain of craters A and B trace the fold axes of adjacent synclines (Fig. 7) and the long axes of the craters are aligned along the synclinal fold hinge. Crater chain C is located near the crest of the anticline between crater chains A and B (Fig. 7). With closer inspection the craters are seen to be composed of linked depressions with complex inter-relationships (Fig. 8).

The craters have been classified into linear, circular, ellipsoidal and elongate end-member geometries. In all types, the long axis of the crater is parallel to the DZ orientation, have flat crater rims and the width of the crater directly corresponds to the width of the underlying DZ. The linear craters are around 200 m wide and have vertical walls 10–20 m deep (Fig. 6b). Circular crater depressions have a diameter ranging from 300 to 700 m and link up with the
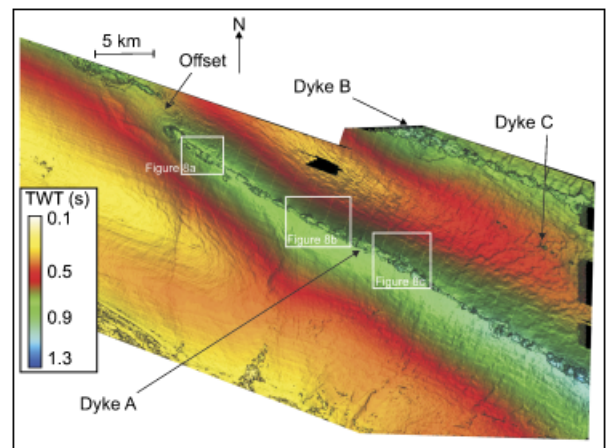
Fig. 7. Top Cretaceous age Chalk time map over the seismic survey. The three dykes are highlighted, trending NW–SE and appear as linear crater chains tracing the synclinal fold axes. The offset geometry of dyke A and the southern synclinal fold axes is highlighted. The hot colours indicate stratigraphic highs and cold colours, lows. Boxes highlight the location of Fig. 8.
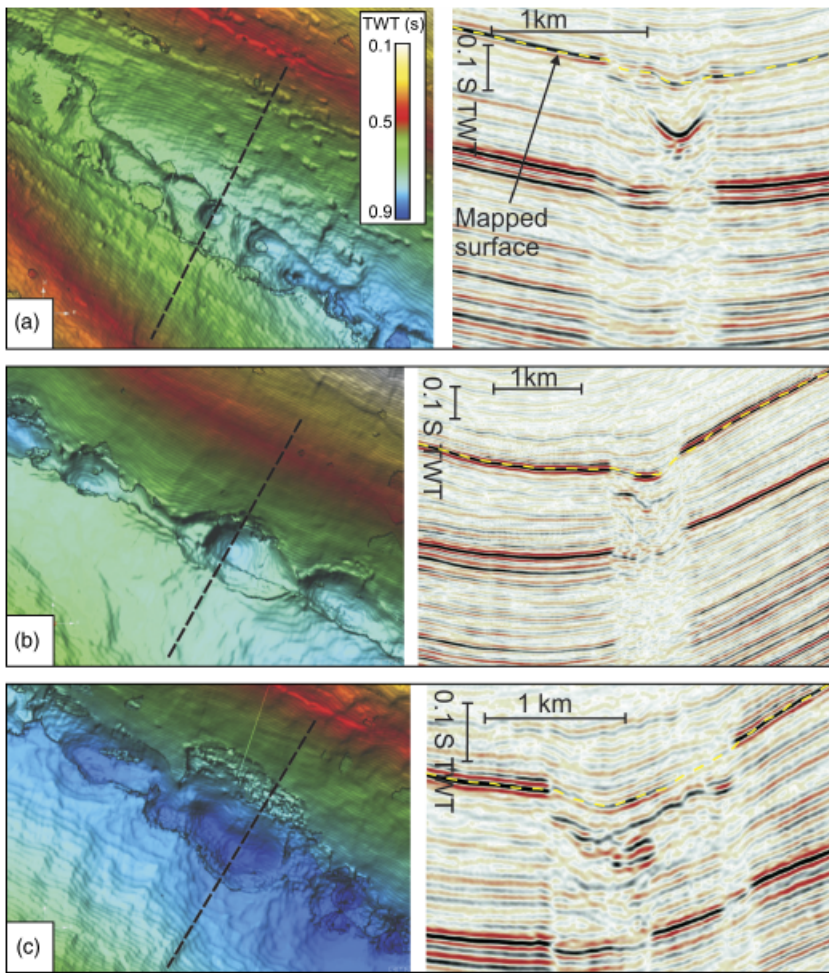
Fig. 8. Close up images of the types of crater found in the survey and corresponding seismic lines through the craters. (a) Seismic line through an elongate crater with an enclosed smaller circular crater. (b) Seismic line through an ellipsoidal crater. (c) Seismic line through a large ellipsoidal crater that has a large underlying triangular diatreme root. Locations are shown in Fig. 7.

linear craters at their lateral tips (Fig. 8b). Ellipsoidal crater depressions are often seen to have coalesced with other smaller ellipsoidal and circular crater depressions (Fig. 8c). Their long axis length is around 1 km and the short axis around 0.5 km. Elongate crater depressions have a similar size range to the ellipsoidal crater depressions but differ in having a more angular rectangular geometry (Fig. 8a). Small circular craters can be found within the larger elongate craters, implying that the small circular craters postdate the larger rectangular craters (Fig. 8a). The largest crater in the data coverage does not fall into any of the described geometries and has an irregular sub-circular shape. Its long axis is 2.5 km and short axis is 2 km; it also has a very complex internal structure where the seismic reflections are broken and discontinuous. Figure 8 shows the range of crater shapes found in the survey and their corresponding vertical DZ.

Interpretation of magnetic data

A high-resolution marine magnetic survey located over the eastern area of the dataset has been used to investigate the DZ imaged by the seismic reflection data. The ULT035 magnetic survey was recorded by Edcon Incorporated and processed by Ark Geophysics in 1990. The magnetic data
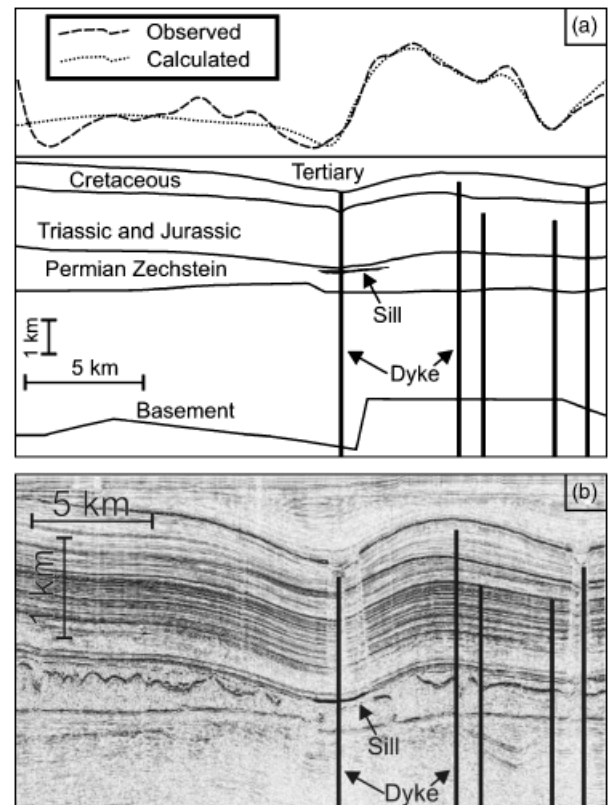
were gridded at a pitch of 500 m and contoured at an interval of 1 nT (nanotelsa) producing a colour shaded relief map (Fig. 9).

The magnetic anomaly map shows two large linear negative anomalies trending NW–SE tracing the synclinal axes and a third smaller linear negative anomaly tracing the crest of the anticlinal axes (Fig. 9). The linear anomalies vary considerably in width along strike, ranging between 2 and 8 km. The linear magnetic anomalies are aligned along the same orientation and position as the linear craters and DZ identified from the seismic reflection data. Each linear negative anomaly (low contours) can be interpreted as the response to a vertically magnetized dyke or dyke system in the dataset and is strong evidence for dykes in the subsurface (Brown *et al.*, 1994). The negative anomalies are the result of the igneous rock being intruded at a time when the Earth's magnetic field was reversed. A magnetic profile orientated perpendicular to the interpreted dyke trend has been modelled using one of the magnetic survey grid lines (Figs 9 and 10). The magnetic model illustrates the comparison of the observed magnetic field and computed magnetic field for a sub-vertical, narrow igneous body rising to 0.8 km below the mean sea level, corresponding to the upper limit of the DZ. To match the observed magnetic field a number of dykes have been interpreted to be
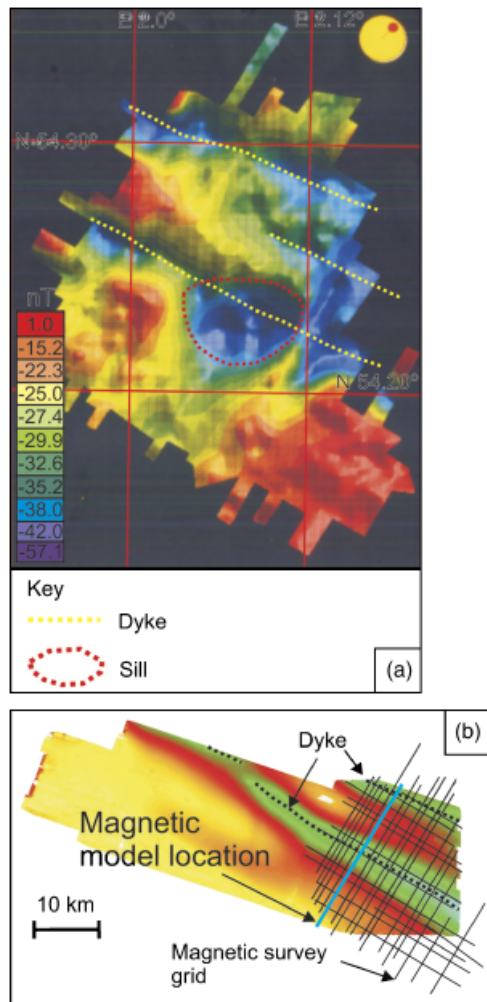
Fig. 9. (a) Magnetic anomaly map over the dataset showing the location and interpretation of the negative magnetic anomalies. (b) Top Cretaceous time map showing the location of the magnetic survey grid in relation to the seismic data coverage.

Fig. 10. (a) Magnetic model showing the observed and calculated magnetic field and the predicted location of igneous material in the dataset. Location of seismic line shown on Fig. 9. (b) Vertical seismic line showing the interpreted location of the dykes and sills in the dataset.

present within the model (Fig. 9). The calculated magnetic field does not correspond with the observed model when two dykes are modelled aligned along the DZ position. Only when more adjacent dykes are added to the model does the calculated field match the observed magnetic field (Fig. 10). In addition to modelling dykes to match the observed magnetic profile we have modelled the presence of an igneous sill (Figs 9 and 10). The variation of width of the linear magnetic anomaly along strike can be interpreted as evidence for the presence of a sill in association with the vertical dykes. Onshore and seismic investigations of igneous plumbing systems of Cenozoic age have found the presence of dykes and sills to be very common and similar sill intrusions have been found in association with dykes in the central North Sea (Smythe, 1994). Although the exact width and height of the igneous bodies cannot be established accurately due to the many different possible outcomes of the modelling, the magnetic data and model clearly demonstrate that igneous dykes and sills are present in the dataset and it is possible that the major-

ity of these igneous bodies are not imaged by seismic reflection data (Fig. 10).

Interpretation

From the seismic observations alone the DZ could be potentially interpreted as a number of different ways. A vertical seismic disturbance is a characteristic of gas chimneys (Løseth *et al.*, 2009). Gas chimneys and shallow gas can be associated with pockmarks at the sea bed or shallow high amplitude reflections indicative of gas deposits (Løseth *et al.*, 2001). Sandstone pipes are also characterized by vertical seismic disturbances and are usually associated with cross cutting of or disruption of stratal reflections (Cartwright 2007, Huuse *et al.*, 2007). In the dataset the DZ do not reach the sea bed, no pockmarks are found on the sea floor and no distinct high-amplitude shallow gas pockets can be identified. The DZ are similar to hydrothermal vent complexes that originate from transgressive sills identified in the Northeast Atlantic margin (Jamtveit *et al.*, 2004; Planke *et al.*, 2005).

Significantly the combination of the DZ imaged in the seismic data and the overlying magnetic anomaly can allow us to confidently interpret the presence of dykes in the dataset, adding to those few dykes previously found in the SNS using these geophysical methods in combination

(Brown *et al.*, 1994, Kirton & Donato 1985). The negative magnetic anomaly is consistent with a dyke or dyke cluster located in the centre of the DZ (Figs 9 and 10). We cannot confidently estimate the dyke width or distinguish between a dyke and a dyke cluster due to the unknown magnetic susceptibility of the igneous material. Using the magnetic model we predict that the most likely location of the dyke or dyke cluster to be within the central disturbance C in the centre of the DZ (Fig. 10).

The downward tapering triangular unit, HA, identified in the seismic data directly overlies what we interpret to be dykes identified by the magnetic data (Figs 6a and 10). The triangular shape of the HA unit and the overlying crater closely resembles surface craters formed by the venting of fluids and diatreme roots created by phreatomagmatic processes (Novikov & Slobodskoy, 1978; Lorenz, 1986; Nemeth *et al.*, 2001 and Jamtveit *et al.*, 2004) (Figs 6a and 8). The HA unit can be interpreted to represent a triangular erosional cavity or diatreme root formed by a phreatomagmatic explosive interaction between basaltic magma, water-saturated sediments and seawater. The linear crater chains overlying the HA unit would in this interpretation mark the upper limit of the diatreme root and would therefore represent the surface expression of the underlying dyke.

The magnetic model cannot predict the width of the dykes present in the dataset; we therefore estimate dyke width to probably be consistent with the average dyke width (1–3 m) from the Mull igneous province (Jolly & Sanderson, 1995) but most likely to be comparable with the onshore Cleveland dyke (average width 20 m) and other 'solitary dykes' originating from the Mull igneous province (Macdonald *et al.*, 1988). Importantly the Cleveland dyke width varies considerably along strike between 5 and 30 m with no systematic variation in width (Macdonald *et al.*, 1988). Moreover dyke width does not correspond to the width of the DZ identified in the seismic data. To explain the width of the DZ the relationship with the magnetic anomaly and the overlying crater must be explored.

Interpretation of the magnetic anomaly does not exclude the possibility of the DZ being composed of one dyke or a linear dyke swarm consisting of numerous anastomosing dykes corresponding to the DZ width (Figs 9 and 10). Importantly, the crater width directly corresponds to the DZ width (Fig. 6), implying a direct relationship.

The DZ consists of three main disturbances that mark a break in reflection continuity, X, Q and Z for wide craters and one main vertical seismic disturbance for a thin DZ (Fig. 6). Using our observations from the seismic and magnetic data, and taking account of the various models of dyke emplacement and maar development, we infer dyke location to be in the centre of the DZ, below the triangular HA (Figs 6, 9 and 10). Therefore, the other observed disturbances within the DZ need to be explained. Since the remaining disturbances, X and Z, consistently underlie the edges of the overlying crater cut into the high velocity Chalk Group, the low velocity Tertiary siliciclastics infilling the crater would result in lateral velocity anomalies being produced from the edges of the crater. The Tertiary siliciclastic crater infill would have a slower seismic velocity than the mainly chalk country rock adjacent to the crater (Fig. 6). A pushdown artefact would therefore result from the fill of low seismic velocity strata, causing the seismic reflections below the crater to be displaced (pushed down) by the thickness of the crater infill. The loss of continuity along strike of the outer disturbances is further evidence that they are indeed seismic artefacts.

Artefacts are vertical features in seismic reflection data (Brown, 1999) and sub-vertical artefacts are generally present due to the processing and migration of the seismic reflection data. The sub-vertical nature of the DZ may directly relate to the inclined dip of the dyke and the effect of the dyke on the surrounding country rock. The reduction of porosity and thermal alteration of the country rock surrounding a sill or dyke is likely to be proportional to the thickness of the igneous body (Einsele *et al.*, 1980). Without any direct evidence that a single dyke, 1–20 m wide, could have had an effect on the adjacent 500 m of country rock we believe that the vertical and sub-vertical DZ are most likely to be seismic artefacts and do not represent real features imaged by seismic reflections. We note that dyke width is considerably smaller than the horizontal seismic resolution. Reprocessing of the seismic reflection data and examination of the near and far seismic datasets would result in a better understanding of the DZ and clearer imaging of the dyke's effect on the seismic reflections.

DISCUSSION

Dyke emplacement and crater chain formation

To our knowledge, dykes have not directly been recognized in detail using 3D seismic reflection data before. Previously only 2D seismic reflection data coupled with magnetic data have provided an understanding of dyke geometry in the subsurface (Kirton & Donato, 1985; Brown *et al.*, 1994). Using 3D seismic reflection data we are able to produce a 3D spatial understanding of dyke emplacement in the SNS.

Dyke emplacement and maar formation can best be studied in areas of recent igneous activity. Significantly, recent igneous events where dykes have been emplaced are rare; only events in Alaska in 1977, Iceland in 1875 and present day California and Afar have been recorded in any detail (Lorenz, 1986; Mastin & Pollard, 1988 and Wright *et al.*, 2006). Importantly eroded and exposed maars and diatremes, and their deposits, allow the study and reconstruction of dyke emplacement and phreatomagmatic processes, (Novikov & Slobodskoy, 1978; Kokelaar, 1986; Lorenz, 1986; Nemeth *et al.*, 2001; Jamtveit *et al.*, 2004 and Svensen *et al.*, 2006) but it is rare to find evidence of a linear dyke with chains of cavities/craters formed by the interaction between magma and water.

The dykes in this study area are most likely to have been emplaced into highly porous unconsolidated Cretaceous
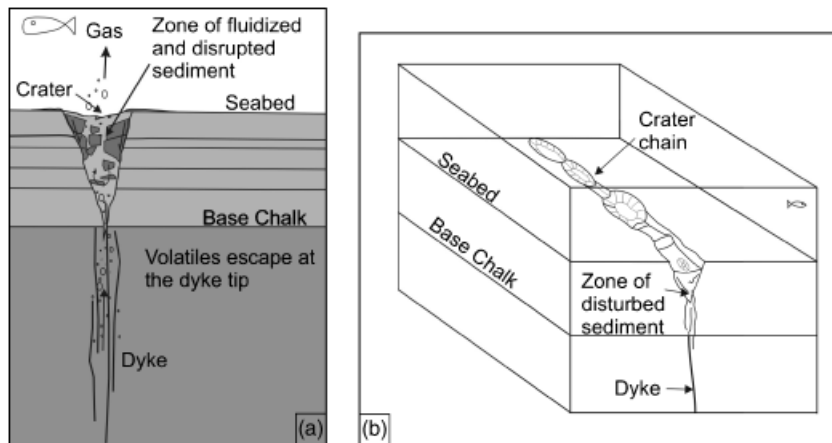
Fig. 11. (a) Schematic model for dyke emplacement and diatreme root formation, based on Lorenz (1986) and Jamtveit *et al.* (2004). (b) Block diagram showing the coalescing nature of the cavities and overlying craters.

age Chalk sediment and Early Tertiary siliclastics near the seabed with porosities ranging from 50% to 70%, (Mallon & Swarbrick, 2002) overlain by a 50–100 m sea water column (Cameron *et al.*, 1992). As the dyke propagate vertically they would encounter host sediments with increasing porosity and this might reasonably have resulted in an increased accumulation of volatiles forming at the propagating dyke tip (Wilson & Head, 2007). As a dyke propagate upwards through the sediment overburden, hot volatiles and gases would escape above the dyke tip inducing fracturing of the country rock (Fig. 11). Escape of the volatiles to the seafloor would create an initial slit-shaped conduit extending up from the dyke tip (Novikov & Slobodskoy, 1978). The conduit wall could have been disrupted by the dynamic effect of the gas explosion velocity, which may reach 100–200 m/s, leading to its certain expansion and decrease in the local hydraulic impedance. This would have caused an increase in the flow velocity and further disruption of the conduit as it transforms from a simple slit to elliptical, circular and finally pipe-like form (Novikov & Slobodskoy, 1978). A cone-shaped cavity can also form near the seafloor in the country rock by the initial explosion caused by the magma–seawater interaction and the overcoming of the confining pressure (Lorenz, 1986). The cavity grows vertically downwards as the confining pressure decreases. Seawater and recycled sediment infill the space created by the explosion. Downward growth is accompanied by lateral expansion of the cavity by gravitational collapse of the cavity/crater wall (Novikov & Slobodskoy, 1978; Lorenz, 1986; Houghton *et al.*, 1999; Nemeth *et al.*, 2001).

The weak cohesive strength of the near surface high porosity Cretaceous chalk and seabed sediments could have facilitated slumping of the margins into the diatreme cavity, creating the triangular shaped high amplitude package identified in the seismic data (Fig. 11). Further recycling of material by magma–water interaction explosions is due to the influx of Chalk aquifer pore water and seawater. Catastrophic loss of pore water and subsequent porosity in the Chalk host sediments by vapourization caused by the hot magma would have led to rapid and localized

compaction around the dyke (Brown *et al.*, 1994). This volume reduction is recorded by the marked thinning of the Cretaceous chalk isopach around the dyke (Fig. 5).

Phreato–magmatic interactions are strictly controlled by the amount of groundwater present; too much water and the eruption is obstructed (Lorenz, 1986; Scott & Wilson, 2002). The optimum ratio of magma : water for maar formation is 3 : 1 (Scott & Wilson, 2002). In a submarine setting the ratio of groundwater to magma may be too high for eruption to take place. If this is the case, it is more likely that the linear craters were formed by magmatic processes involving juvenile volatiles escaping from the dyke tip. As the dyke tip stalls, gases and volatiles rising through the magma congregate at tip of the dyke forming a gas cap. The leakage of the gas cap to the surface results in the collapse of the overlying country rock into the void created and the formation of a collapse crater at the surface (Scott & Wilson, 2002; Svensen *et al.*, 2006).

The variation in crater size, geometry and the presence or absence of a diatreme feeder root (HA unit) over a short distances identified in the seismic data is intriguing (Fig. 7). Larger craters found in the dataset that have a triangular cavity above the dyke (Fig. 8c) are most likely the result of a water vapour explosion caused by the interaction between magma and seawater, creating a diatreme like root which contains slumped and reworked material (Fig. 11a and b). The thinner linear craters (Fig. 6b) do not have a cavity beneath them and are the result of collapse of surface rocks into the space vacated by the leakage of gas which has accumulated at the top of a dyke. Larger elongate craters that contain smaller circular craters (Figs 8a and 11b) are most likely the result of further degassing of the magma after the initial cavity is formed. Long-term venting of volatiles may continue for a significant period of time after the creation of the main cavity. The coalescing of the craters indicates that craters developed independently of each other, joining together during crater growth.

Lateral variation in dyke height and width may control crater size at the seabed. Higher areas of relief along the lateral dyke tip may focus the amount of magma volatiles leading to higher rates of ascent and greater country rock

fracturing. Vertical and lateral fingering of the dyke tip may also produce a wide zone of magmatic and country rock interaction near the seabed and account for the range of collapse pits in the dataset (Figs 8 and 11). We assume that the oldest craters are the largest as the longer the duration of explosive activity, the larger the depth and diameter of the crater and associated diatreme (Lorenz, 1986). The advantage of 3D seismic reflection data is that we can follow the evolution of dyke emplacement in the SPB using this scaling relationship.

No maar ejecta beds can be identified adjacent to the craters. This may be the result of the size of the initial cavity formed. A large initial cavity and rapid loss of porosity from the country rock would result in any extrusive material being constrained within a large cavity. The thickness of ejecta beds range from <10 m to >40 m (Lorenz, 1986). Thus, it is highly likely that any ejecta beds deposited are below seismic resolution and cannot be imaged. Regional well analysis has identified numerous tuff and pyroclastic ejecta beds in SNS hydrocarbon and BGS bore holes in the Thanetian, (Morton & Knox, 1990) this being the first evidence for Tertiary pyroclastic sedimentation. A thick tuff layer within the early Tertiary strata has been discovered in a recent hydrocarbon well, 43/19a-C1.

Timing of dyke emplacement

The timing of igneous activity is important to further understand the role of the Tertiary igneous province in basin evolution in the SPB. Sediments onlapping onto the Cretaceous age Chalk and Lower Tertiary age rocks date the formation of the craters overlying the dyke and therefore dyke emplacement. Owing to the lack of detailed well control we cannot date these onlapping sediments with accuracy. We can observe that the date is probably Late Palaeocene–Early Eocene (58–54 Ma) due to the fact that the onlapping sediments lie close to the Cretaceous Tertiary boundary where early Eocene age tuffs have been found in regional (within 20 km) hydrocarbon exploration wells and that similar Late Palaeocene igneous activity has been well documented in the Vøring and Møre basins (Lott & Knox, 1994; Svensen *et al.*, 2003; Jamtveit *et al.*, 2004; Planke *et al.*, 2005 and Wall *et al.*, 2008) (Fig. 6). The negative magnetic anomaly of the dyke indicates that the dykes were intruded at a time when the Earth's magnetic field was reversed. Reversal of the Earth's magnetic field occurred in the Early Tertiary at 63, 58 and 56 Ma (Cande & Kent, 1995), thus loosely constraining the timing of dyke emplacement to one of these periods.

The trend of the SPB dykes aligns with the offshore dykes identified by Kriton & Donato (1985) and with the onshore Acklington, Blythe and Cleveland dykes that originate from the Mull igneous centre (Kirton & Donato, 1985; Brown *et al.*, 1994) (Fig. 12). Emplacement of the Cleveland dyke has been dated at 58.4 ± 1.1 Ma (Macdonald *et al.*, 1988). This date corresponds to the Early Tertiary reversal in the Earth's magnetic field, matching the magnetic anomaly (Fig. 9). We predict that the dykes in our
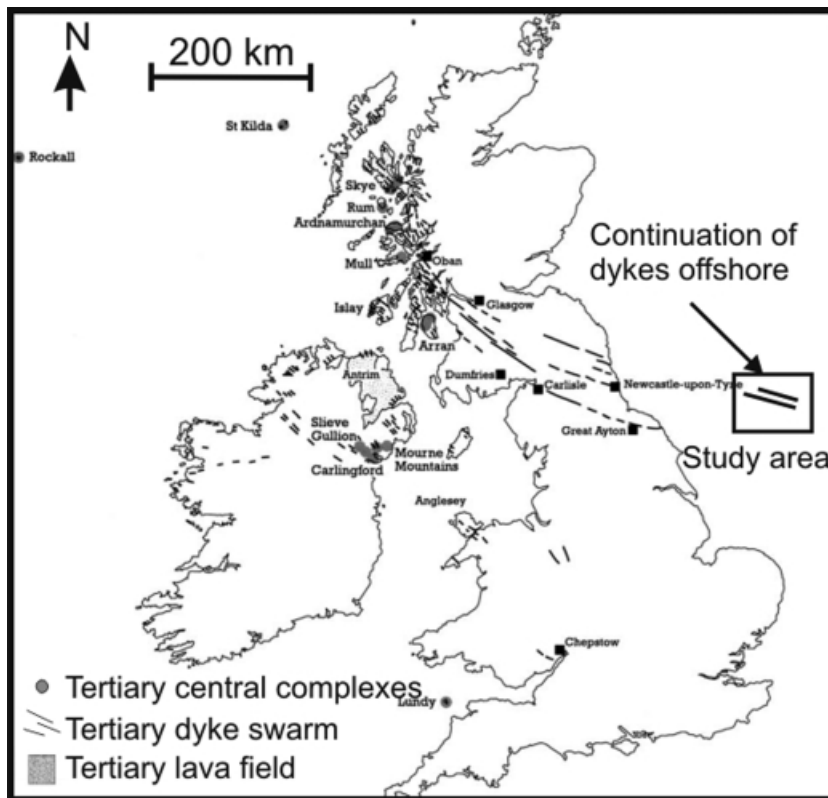

Fig. 12. Map of the British Tertiary volcanic province. The map shows the location of the dykes mapped in the SPB and their correlation with the onshore dykes in the NE of England. From Emeleus (1982).

dataset are part of the Tertiary igneous province and are most likely the same age as the Cleveland dyke and the associated igneous activity in the Norwegian Møre and Vøring basins, therefore giving a date for dyke emplacement in the Late Paleocene, 58 Ma.

Tertiary Igneous Province

The emplacement of the dyke swarm into the SPB is significant for the understanding of the evolution of the Tertiary igneous province. The position of the dyke buoyancy level is unknown, but we can observe that the dyke laterally propagated hundreds of kilometres into the SPB basin (Fig. 12). The dykes have the same trend as regional basement lineaments in the SPB. Depending at what stratigraphic level the dyke was emplaced; the dyke could have exploited basement weaknesses or their orientation parallel to basement structures could be a coincidence. The recognition of dykes in the SPB furthers the known extent of the Tertiary igneous province (Kirton & Donato, 1985; Brown *et al.*, 1994) (Fig. 12).

Morton & Knox (1990) found over 200 tephra layers in the Late Paleocene and Early Eocene in the North Sea basin and found that the tephras were generated by hydroclastic processes. Morton & Knox (1990) stated that the origin of the highly explosive eruption is uncertain and that water magma interaction may have occurred all along the entire 2000 km length of the proto NE Atlantic margin and is potentially source related. The dykes in the SPB are potential sources for tephra layers in local wells (e.g. BGS borehole 81/46 A, Morton & Knox, 1990). Any tephras produced by the SPB dykes could be transported over vast distances by sea water currents. Assuming that all dykes emplaced as a result Tertiary igneous province interacted with groundwater or seawater and resulted in explosive maar formation or the creation of hydrothermal vents, vast amounts of explosive tephra and ash would be produced and deposited all over the North Sea Basin. Because of extensive uplift and erosion of the NE Atlantic margin (Scotland and Northern England), the dykes and igneous centres are now exposed on the Earth's surface, resulting in all traces of maar and explosive activity being eroded away from the Tertiary igneous province. Only in the SPB, West of Shetland and in the Norwegian Møre and Vøring basins, where burial has preserved the dykes and maar craters, evidence for explosive magma–water interactions still exists (Skogseid *et al.*, 2000; Jamtveit *et al.*, 2004).

Relationship between folding and dyke emplacement

The close spatial correspondence between the position of the dykes and the synclinal fold axis trends in the SPB is remarkable. In our dataset and in previous studies dykes in the SNS have been found to trace synclinal fold axes (Kirton & Donato, 1985; Brown *et al.*, 1994). The offset geometry of dyke A (Fig. 7) traces the offset geometry of the synclinal axes. This relationship is evidence of the control of dyke location on fold axes. The emplacement of the

dykes significantly pre dates the Late Eocene–Oligocene (33–28 Ma) onset of regional folding in the SNS (Ziegler, 1981; Hughes & Davison, 1993). We interpret the dykes to have acted as strong vertical partitions in the basin crossing the basal detachment for the detachment buckle folds. Strata between the dyke partitions were buckled by compressional flexural slip, resulting in the dykes defining the position of the synclinal axes (Fig. 13). The main compressional stress must be perpendicular to the pin/dyke orientation for this scenario to occur. At the onset of folding the basin was tilted to the NE and uplifted in the SW due to inversion of the SPT (Van Hoorn, 1987). Gravitational collapse of the salt overburden towards the NE formed long wavelength buckle folds with axes trending NW–SE (Fig. 2) (Stewart & Coward, 1995) perpendicular to the dyke direction. Alternatively the dykes could act as regional weaknesses in the basin forming nucleation points for fold growth.

Martian pit chain craters

The linear craters identified above the DZ are very similar to Martian pit chain craters imaged by remote sensing (Figs 8 and 14). We recognize the linear craters imaged in our survey to be pit chain craters following the criteria of Wyrick *et al.* (2004), where pit chain craters are classified as circular to elliptical depressions found in alignment (chains), which in many cases coalesce into linear troughs. Pit chain craters lack an elevated rim, ejecta deposits, or lava flows that are associated with impact craters or calderas (Wyrick *et al.*, 2004); criteria that are met in our dataset.

Pit chain craters are rare on earth (Ferrill *et al.*, 2004), making our observations important to furthering the understanding of pit chain formation on Earth, Mars and other planetary bodies. The debate on the origin of pit chain craters is held back by the lack of an Earth analogue, and to date up to eight different origins have been
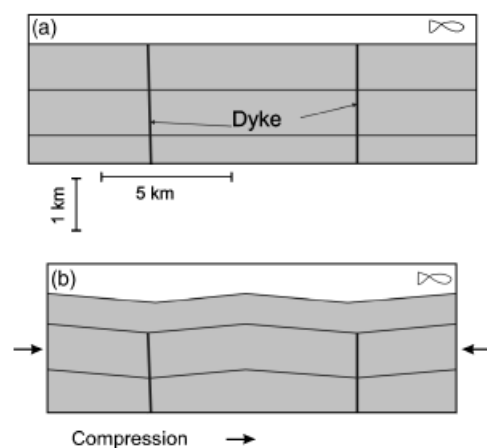
Fig. 13. Model showing the role of dykes in fold development and growth. (a) The dykes are emplaced into the basin up to the seabed. (b) The dykes act as partitions in the basin. During regional compression the strata between the partitions fold by flexural slip while the dykes act as lateral struts.

Fig. 14. THEMIS image of Martian pit chain craters (image V03749003, Christensen *et al.*).

proposed for pit chain crater formation on Mars (Wyrick *et al.*, 2004). Our recognition of pit chain craters in the SPB, buried in the subsurface, provides a new Earth analogue for pit chain craters on Mars. We recognize that the SPB pit chain craters are formed by the release of volatiles during dyke emplacement. This gives further support towards the theory that pit chain craters on Mars are formed by the same igneous processes identified in the SPB.

The proposed Silverpit impact crater

The Silverpit crater is a proposed impact structure located 20 km to the south of the study area (Fig. 1). An igneous alternative origin for the Silverpit structure has been suggested but despite all the controversy surrounding its origin, this has not been explored (Stewart & Allen, 2004). Before the 1960s the majority of impact structures

were considered to have an igneous cryptovolcanic origin (Price, 2001). Leaking of volatiles from a sill at depth has been found to create large 5 km wide craters in the Atlantic margin (Svensen *et al.*, 2004). A similar scenario can be put forward for the Silverpit crater. The Silverpit crater does not have a vertical seismic disturbance beneath the centre of the crater, but a narrow conduit could still transport volatiles to the seabed. However the Silverpit crater formation has been dated in the mid-Eocene (45 Ma) (Wall *et al.*, 2008). The younger age of the Silverpit crater compared to the timing of igneous activity in the SPB and critically the lack of a magnetic and gravity anomaly beneath the Silverpit crater thus appears to rule out an igneous origin for the Silverpit crater.

CONCLUSIONS

(1) Three buried dykes have been identified and mapped in the SPB subsurface using 3D seismic reflection and magnetic data. Magnetic modelling indicates the presence of further dykes not imaged by seismic data. This is attributable to the dykes not reaching the seabed and causing collapse or explosive interaction with porewater thus producing the distinct seismic disturbances imaged.

(2) Emplacement resulted in localized dewatering and collapse of the country rock above the dyke tip. Volatiles escaped above the dyke tip due to the interaction between magma and aquifer pore water. Explosive phreatomagmatism and release of volatiles have resulted in the creation of diatremes and collapse craters above the dyke tips. The craters above the dykes have coalesced into linear crater chains. The variation in crater size and crater interaction has been interpreted to represent different magma–water interaction processes and possible variation in dyke width and height along strike.

(3) The synclinal fold axes of regional salt-cored detachment folds trace the dykes in the study area. We interpret the dykes as rigid linear struts that control the location and wavelength of Late Eocene–Oligocene folds.

(4) Magnetic anomaly maps over the SPB and the timing of dyke emplacement rule out an igneous origin for the Silverpit crater.

(5) The dykes identified in the SPB form part of extensive Tertiary igneous province. The dykes are estimated to have an age of 58 Ma.

(6) The dykes identified in the SPB are a new Earth analogue to Martian pit chain craters. The SPB dykes show that pit chain craters can be formed above dyke tips, giving further support for an igneous origin for the Martian pit chain craters.

(7) 3D seismic reflection data coupled with magnetic data form a powerful tool to map and understand magmatic intrusion into the Earth's crust.

ACKNOWLEDGEMENTS

REFERENCES

BAILEY, J.B., ARBIN, P., DAFFINOTI, O., GIBSON, P. & RITCHIE, J.S. (1993) Permo-Carboniferous plays of the Silver Pit Basin. In: *Petroleum Geology of Northwest Europe: Proceedings of the 4th Conference* (Ed. by J.R. Parker), pp. 707–715. The Geological Society, London.

BROWN, A.R. (1999) *Interpretation of Three-Dimensional Seismic Data, 5th edition. AAPG Memoir 42.* Tulsa, Oklahoma, pp. 514.

BROWN, G., PLATT, N.H. & MCGRANDLE, A. (1994) The geophysical expression of tertiary dykes in the southern North Sea. *First Break*, **12**(3), 137–146.

CAMERON, T, D, J., CROSBY, A., BALSON, P.S., JEFFERY, D.H., LOTT, G.K., BULAT, J. & HARRISON, D.J. (1992) *United Kingdom Offshore Regional Report: the Geology of the Southern North Sea.* HMSO for the British Geological Survey, London.

CANDE, S.C. & KENT, D.V. (1995) Revised calibration of the geomagnetic polarity timescale for the Late Cretaceous and Cenozoic. *Journal of Geophysical Research, B, Solid Earth and Planets.*, **100**, 6093–6095.

CARTWRIGHT, J.A., HUUSE, M. & APLIN, A. (2007) Seal bypass systems. *AAPG Bulletin*, **91**, 1141–1166.

CHEVALLIER, L. & WOODFORD, A. (1999) Morpho-tectonics and mechanism of emplacement of the dolerite rings and sills of the western Karoo, South Africa. *S. Afr. J. Geol.*, **102**, 43–54.

CHRISTENSEN, P.R., GORELICK, N.S., MEHALL, G.L. & MURRAY, K.C. THEMIS Public Data Releases, Planetary Data System node, Arizona State University. Available at http://themis-data.asu.edu (accessed 1 October 2006).

COWARD, M. & STEWART, S. (1995) Salt-influenced structures in the Mesozoic-Tertiary cover of the southern North Sea, U.K. In: *Salt Tectonics: A Global Perspective* (Ed. by M.P.A. Jackson, D.G. Roberts & S. Snelson), *AAPG Memoir 65*, pp. 229–250.

COWARD, M.P. (1993) The effect of late Caledonian and Variscan continental escape tectonics on basement structure, Paleozoic basin kinematics and subsequent Mesozoic basin development in NW Europe. In: *Petroleum Geology of Northwest Europe: Proceedings of the 4th Conference* (Ed. by J.R. Parker), pp. 1095–1108. Geological Society, London.

DAVIES, R.J., STEWART, S.A., CARTWRIGHT, J.A., LAPPIN, M., JOHNSTON, R., FRASER, S.I. & BROWN, A.R. (2004) 3D seismic technology; are we realising its full potential? *Mem. Geol. Soc. Lond.*, **29**, 1–9.

DUTOIT, A.I. (1920) The Karoo dolerites. *Trans. Geol. Soc. South Africa*, **33**, 1–42.

EINSELE, G., GIESKES, J.M., CURRAY, J., MOORE, D.M., AGUAYO, E., AUBRY, M.P., FORNARI, D., GUERRERO, J., KASTNER, M., KELTS, K., LYLE, M., MATOBA, Y., MOLINA, C.A., NIEMITZ, J., RUEDA, J., SAUNDERS, A., SCHRADER, H., SIMONEIT, B. & VACQUIER, V. (1980) Intrusion of basaltic sills into highly porous sediments, and resulting hydrothermal activity. *Nature (London)*, **283**, 441–445.

EMELEUS, C.H. (1982) Tertiary igneous activity: the central complexes (British Isles). In: *Igneous Rocks of the British Isles* (Ed. by D.S. Sutherland), pp. 269–414. Wiley, Chichester.

FERRILL, D.A., WYRICK, D.Y., MORRIS, A.P., SIMS, D.W. & FRANKLIN, N.M. (2004) Dilational fault slip and pit chain formation on Mars. *GSA Today*, **14**, 4–12.

GEORGE, G.T. & BERRY, J.K. (1997) Permian (upper Rotliegend) synsedimentary tectonics, basin development and palaeogeography of the southern North Sea. *Geol. Soc. Spec. Publ.*, **123**, 31–61.

GOULTY, N.R. (2005) Emplacement mechanism of the Great Whin and Midland Valley dolerite sills. *J. Geol. Soc. Lond.*, **162**, 1047–1056.

HANSEN, D.M. & CARTWRIGHT, J. (2006) Saucer-shaped sill with lobate morphology revealed by 3D seismic data; implications for resolving a shallow-level sill emplacement mechanism. *J. Geol. Soc. Lond.*, **163**(3), 509–523.

HANSEN, D.M., CARTWRIGHT, J.A. & THOMAS, D. (2004) 3D seismic analysis of the geometry of igneous sills and sill junction relationships. *Mem. Geol. Soc. Lond.*, **29**, 199–208.

HITCHEN, K. & RITCHIE, J.D. (1987) Geological review of the West Shetland area. In: *Petroleum Geology of North West Europe* (Ed. by J. Brooks & K.W. Glennie), pp 737–749. Graham and Trotman, London.

HITCHEN, K. & RITCHIE, J.D. (1993) New K-Ar ages, and a provisional chronology for the offshore part of the British Tertiary Igneous Province. *Scott. J. Geol.*, **29**, 599–624.

HOUGHTON, B.F., WILSON, C.J.N. & SMITH, I.E.M. (1999) Shallow-seated controls on styles of explosive basaltic volcanism; a case study from New Zealand. *J. Volcanol. Geotherm. Res.*, **91**, 97–120.

HUGHES, M. & DAVISON, I. (1993) Geometry and growth kinematics of salt pillows in the southern North Sea. *Tectonophysics*, **228**, 239–254.

HUUSE, M., CARTWRIGHT, J.A., HURST, A. & STEINSLAND, N. (2007) Seismic characterisation of large-scale sandstone intrusions. In: *Sand Injectites: Implications for Hydrocarbon Exploration and Production* (Ed. by A. Hurst & J.A. Cartwright), *AAPG Memoir 87*, 21–35.

JAMTVEIT, B., SVENSEN, H., PODLADCHIKOV, Y.Y. & PLANKE, S. (2004) Hydrothermal vent complexes associated with sill intrusions in sedimentary basins. In: *Physical Geology of High-Level Magmatic Systems*, Vol. 234 (Ed. by C. Breitkreuz & N. Petford), pp. 233–241. Geological Society Special Publications, London.

JOLLY, R.J.H. & SANDERSON, D.J. (1995) Variations in the form and distribution of dykes in the Mull swarm, Scotland. *Journal of Structural Geology.*, **17**, 1543–1557.

KIRTON, S.R. & DONATO, J.A. (1985) Some buried Tertiary dykes of Britain and surrounding waters deduced by magnetic modelling and seismic reflection methods. *J. Geol. Soc. Lond.*, **142**, 1047–1057.

KOKELAAR, B.P. (1982) Fluidization of wet sediments during the emplacement and cooling of various igneous bodies. *J. Geol. Soc. Lond.*, **139**, 21–33.

KOKELAAR, P. (1986) Magma – water interactions in subaqueous and emergent basaltic volcanism. *Bull. Volcanol.*, **48**, 275–289.

LORENZ, V. (1986) On the growth of maars and diatremes and its relevance to the formation of tuff rings. *Bull. Volcanol.*, **48**, 265–274.

LØSETH, H., GADING, M. & WENSAAS,. (2009) Hydrocarbon leakage interpreted on seismic data. *Marine and Petroleum Geology*, **26**, 1304–1319.

LOTT, G.K. & KNOX, R.W.O'B. (1994) Post-Triassic of the southern North Sea. In: *Lithostratigraphic Nomenclature of the UK North Sea*, **Vol. 7** (Ed. by R.W.O'B. Knox & W.G. Cordey) British Geological Society, Keyworth, Nottingham.

MACDONALD, R., WILSON, L., THORPE, R.S. & MARTIN, A. (1988) Emplacement of the Cleveland Dyke; evidence from geochemistry, mineralogy, and physical modelling. *J. Petrol.*, **29**, 559–583.

MALLON, A.J. & SWARBRICK, R.E. (2002) A compaction trend for non-reservoir North Sea Chalk. *Mar. Petrol. Geol.*, **19**, 527–539.

MASTIN, L.G. & POLLARD, D.D. (1988) Surface deformation and shallow dike intrusion processes at Inyo Craters, Long Valley, California. *J. Geophys. Res., B, Solid Earth Planets*, **93**(0885–3401), 13,221–13,235.

MORTON, A.C. & KNOX, R.W.O.B. (1990) Geochemistry of late Palaeocene and early Eocene tephras from the North Sea Basin. *J. Geol. Soc. Lond.*, **147**(0016–7649), 425–437.

NEMETH, K., MARTIN, U. & HARANGI, S. (2001) Miocene phreatomagmatic volcanism at Tihany (Pannonian Basin, Hungary). *J. Volcanol. Geothermal Res.*, **111**, 111–135.

NOVIKOV, L.A. & SLOBODSKOY, R.M. (1978) Mechanism of formation of diatremes. *International Geology Review*, **21**, 1131–1139.

PLANKE, S., RASMUSSEN, T., REY, S.S. & MYKLEBUST, R. (2005) Seismic characteristics and distribution of volcanic intrusions and hydrothermal vents complexes in the Vøring and Møre basins. In: *Petroleum Geology: North-West Europe and Global Perspectives-Proceedings of the 6th Petroleum Geology Conference* (Ed. by A.G. Doré & B. Vining), pp. 833–844. Geological Society, London.

PRICE, N.J. (2001) *Major Impacts and Plate Tectonics*. Routledge, London.

SCOTT, E.D. & WILSON, L. (2002) Plinian eruptions and passive collapse events as mechanisms of formation for Martian pit chain craters. *J. Geophys. Res., E, Planets*, **107**, 12.

SIMM, R. & WHITE, R. (2002) Phase, polarity and the interpreter's wavelet. *First Break*, **20**(5), 277–281.

SKOGSEID, J., PLANKE, S., FALEIDE, J.L., PEDERSEN, T., ELDHOLM, O. & NEVERDAL, F. (2000) NE Atlantic continental rifting and volcanic margin formation. In: *Dynamics of the Norvegian Margin*, **Vol. 167** (Ed. by A. Nottvedt), pp. 295–326. Geological Society Special Publications, London.

SMYTHE, D.K. (1994) Geophysical evidence for ultrawide dykes of the Late Carboniferous quartz-dolerite swarm of northern Britain. *Geophys. J. Int.*, **119**, 20–30.

STEWART, S.A. & ALLEN, P.J. (2004) Earth science – an alternative origin for the 'Silverpit crater' – reply. *Nature*, **428**(6980), U2–U2.

STEWART, S.A. & COWARD, M.P. (1995) Synthesis of Salt Tectonics in the Southern North-Sea, UK. *Mar. Petrol. Geol.*, **12**(5), 457–475.

SVENSEN, H., JAMTVEIT, B., PLANKE, S. & CHEVALLIER, L. (2006) Structure and evolution of hydrothermal vent complexes in the Karoo Basin, South Africa. *J. Geol. Soc., Lond.*, **163**, 671–682.

SVENSEN, H., PLANKE, S., JAMTVEIT, B. & PEDERSEN, T. (2003) Seep carbonate formation controlled by hydrothermal vent complexes: a case study from the Vøring Basin, the Norwegian Sea. *Geo-Mar. Lett.*, **23**, 351–358.

SVENSEN, H., PLANKE, S., MALTHE, S.A., JAMTVEIT, B., MYKLEBUST, R., RASMUSSEN, E.T. & REY, S.S. (2004) Release of methane from a volcanic basin as a mechanism for initial Eocene global warming. *Nature (London)*, **429**, 542–545.

TRUDE, K.J. (2004) Kinematic indicators for shallow level igneous intrusions from 3D seismic data; evidence of flow direction and feeder location. *Mem. Geol. Soc. Lond.*, **29**, 209–217.

VAN HOORN, B. (1987) Structural evolution, timing and tectonic style of the Sole Pit inversion. *Tectonophysics.*, **137**, 239–284.

WALL, M.L.T., CARTWRIGHT, J. & DAVIES, R.J. (2008) An Eocene age for the proposed Silverpit impact crater. *J. Geol. Soc., Lond.*, **165**, 781–794.

WILSON, L. & HEAD, J.W. (2007) An integrated model of kimberlite ascent and eruption. *Nature*, **447**(7140), 53–57, doi: 10.1038/nature05692.

WRIGHT, T.J., EBINGER, C., BIGGS, J., AYELE, A., YIRGU, G., KEIR, D. & STORK, A. (2006) Magma-maintained rift segmentation at continental rupture in the 2005 Afar dyking episode. *Nature*, **442**, 291–294.

WYRICK, D., FERRILL, D.A., MORRIS, A.P., COLTON, S.L. & SIMS, D.W. (2004) Distribution, morphology, and origins of Martian pit crater chains. *J. Geophys. Res., E, Planets*, **109**, 6.

ZIEGLER, P.A. (1981) Evolution of sedimentary basins in North-West Europe. In: *Petroleum Geology of the Continental Shelf of N.W. Europe* (Ed. by L.V. Illing & G.D. Hobson), pp. 76–84. Institute of Petroleum, London.